Anisotropic strain, magnetic properties, and lattice dynamics in self-assembled multiferroic CoFe2O4-PbTiO3 nanostructures

C. Y. Tsai, H. R. Chen, F. C. Chang, H. H. Kuo, H. M. Cheng, W. C. Tsai, Y. H. Chu, C. H. Lai, and W. F. Hsieh

Citation: Journal of Applied Physics **115**, 134317 (2014); doi: 10.1063/1.4870803
View online: http://dx.doi.org/10.1063/1.4870803
View Table of Contents: http://scitation.aip.org/content/aip/journal/jap/115/13?ver=pdfcov
Published by the AIP Publishing

Anisotropic strain, magnetic properties, and lattice dynamics in self-assembled multiferroic $CoFe_2O_4$-$PbTiO_3$ nanostructures

C. Y. Tsai,[1] H. R. Chen,[1] F. C. Chang,[2,3] H. H. Kuo,[2] H. M. Cheng,[3] W. C. Tsai,[4] Y. H. Chu,[2] C. H. Lai,[4] and W. F. Hsieh[1,a)]
[1]*Department of Photonics and Institute of Electro-Optical Engineering, National Chiao Tung University, 1001 Tahsueh Rd., Hsinchu 300, Taiwan*
[2]*Department of Materials Science and Engineering, National Chiao Tung University, Hsinchu 31040, Taiwan*
[3]*Material and Chemical Research Laboratories, Industrial Technology Research Institute, Hsinchu 310, Taiwan*
[4]*Department of Materials Science and Engineering, National Tsing Hua University, Hsinchu 31013, Taiwan*

(Received 16 February 2014; accepted 26 March 2014; published online 7 April 2014)

We investigate the anisotropic stress dependent magnetic and phonon behaviors in self-assembled $CoFe_2O_4$-$PbTiO_3$ (CFO-PTO) nanostructures deposited on $SrRuO_3$ buffered $SrTiO_3$ substrates of various thickness. The increased vertical compressed stress with increasing thickness enhances the vertical magnetic anisotropy of CFO while gradually reducing the vertical polarization of PTO. By applying the magnetic-field dependent Raman scattering, the CFO-A_{1g} and $T_{2g}(1)$ phonon frequencies shift oppositely because of the magnetostriction. Moreover, the PTO-A_1 mode intensities anomalously enhance and the A_1 and E mode frequencies, respectively, increase and decrease, which prove the existence of the stress-mediated magnetoelectric (ME) effect. This study shows that the ME transmission process is dominated by interfacial stress, which is critical for enhancing the ME efficiency. © *2014 AIP Publishing LLC*. [http://dx.doi.org/10.1063/1.4870803]

I. INTRODUCTION

Self-assembled spinel-perovskite multiferroic materials with the coexistence of the ferromagnetic and ferroelectric properties attract great research interests because of the magnetoelectric (ME) effect.[1–3] The ME effect involves three processes.[1,4] First, the spinel materials generates stress under an applied magnetic field owing to magnetostriction. Second, the stress is transmitted to the surrounding perovskite materials through interfacial coupling. Finally, the polarizations are produced from the strained perovskite materials.[1,4] Similarly, the converse ME effect describes the modification of magnetization by application of an electric field.[5] The degree of stress transmission through the spinel-perovskite interfaces is strongly correlated with the interfacial stress and the binding of two phases. Recently, the first-principles-based calculations have shown that the ME strength can be enhanced by tuning the biaxial strain in ferroelectric/ferromagnetic bi-layer systems.[6,7] For self-assembled nanostructures, the calculation shows that their ME strengths could either be enhanced by the increased elastic interaction[4] and residual stress[8] or be reduced by the substrate clamping effect.[9] Therefore, a lattice-compatible substrate[10] or a high aspect ratio for nano-pillars[9] has been proposed to minimize substrate constrains. However, the influences of interfacial stress and the rod aspect ratio on the ME strengths of composite nanostructures remain experimentally unclear. This is because the leakage problems[2,3] and the small ME signals[11,12] make the ME measurements of nanostructures difficult. Because a stress-mediated ME process should disturb the lattice dynamics, the magnetic-field dependent Raman scattering is used to probe the ME interaction.[13] Furthermore, the degree of ferroelectric phonon shift is demonstrated proportional to the ME strength of bi-layer films,[14] which provides a nondestructive method of investigating the ME effect of nanostructures.

In our previous report,[15] we have demonstrated that the magnetostriction exists in $CoFe_2O_4$-$PbTiO_3$ (CFO-PTO) nanostructures on MgO substrate by examining the CFO-A_{1g} phonon frequency variations under the magnetic-field dependent Raman scattering. However, the ME effects were not observed owing to the superposition of phonons. Therefore, in this work, we further investigate the ME coupling of CFO-PTO by using the polarized Raman scattering to separate the ferroelectric phonons from spinel ones. The stress dependent magnetic anisotropies, phonons, and ME coupling are studied in CFO-PTO nanostructures of various thicknesses from 17 to 205 nm, corresponding to CFO rod aspect ratios of 0.85 to 10.3 embedded in a PTO matrix, on $SrRuO_3$ (SRO) buffered $SrTiO_3$ (STO) substrates. We found that, to enhance the ME strength, the efficient stress transmission mediated by interfacial stress is more critical than the magnetostriction increased by the rod aspect ratio.

II. EXPERIMENTAL DETAILS

CFO-PTO films were deposited on $SrRuO_3$ buffered $SrTiO_3$(001) substrates by pulsed laser deposition (PLD) using a composite target of $(CoFe_2O_4)_1$-$(PbTiO_3)_2$ at 600 °C under an oxygen pressure of 100 mtorr. X-ray diffraction (XRD) measurements were conducted using a high-resolution four-circle X-ray diffractometer (HRXRD, Bede D1) with *Cu-kα*$_1$ radiation. Sample topography and polarization were characterized using piezoelectric force microscopy (PFM, Veeco Escope).[15] A magnetic hysteresis loop was recorded using a vibrating

a)Author to whom correspondence should be addressed. Electronic mail: wfhsieh@mail.nctu.edu.tw

sample magnetometer (VSM, Princeton 3900) at RT. Polarized micro-Raman scattering was recorded through a microscope of NA = 0.9 using an iHR550 LabRam Jobin-Yvon spectrometer with a grating of 1800 g/mm under 532 nm excitation. The $Z(XX)\bar{Z}$ and $Z(XY)\bar{Z}$ configurations corresponded to backscattering configurations with parallel and crossed polarizations, respectively.

III. RESULTS AND DISCUSSION

Figure 1(a) shows the diffraction peaks of PTO(002) and CFO(004) near 40° to 47° for the epitaxial films[16] of different thicknesses on high quality SRO thin-film buffered STO substrates. Figure 1(b) shows the CFO lattice constants and bulk value (CFO: $a = 8.38$ Å). CFO rods are generally in-plane elongated and out-of-plane compressed when embedded in a perovskite matrix.[3,15,17,18] However, CFO of 17 nm film is in-plane compressed. For ultra-thin spinel-perovskite materials, in-plane compressive stress seems to dominate in CFO.[19] Because the in-plane compressive stress develops in pure CFO thin-films up to a critical thickness of 40 to 150 nm on STO[20] or SRO buffered STO[21] substrates, the in-plane strain on thinner multiferroic materials is ascribed to the substrate effect. As thickness increased from 17 nm to 85 nm, the out-of-plane lattice constant decreased from 8.378 Å to 8.355 Å. It shows the in-plane compression transfers to an out-of-plane compressive stress. This implies that the stress from PTO phase dominates in 85 nm films. The stress then is partially relaxed as the thickness increased to 205 nm. For self-assembled materials, strain can be released by increasing the growth temperature[17] or the film thickness.[18] Approximate 0.1% strain relaxation on CFO is observed in CFO-PTO films as the thickness increased from 85 nm to 205 nm.

The splitting of PTO (002) diffraction peaks near 44° to 45.8° in Fig. 1(a) shows the existence of two PTO domains, labeled as domains c_1 and c_2. These domains are confirmed as vertically polarized by the out-of-plane PFM phase image in the inset of Fig. 1(a), where the white and black regions correspond to the alternative up and down polarizations, respectively. Formation of c-domains expands the larger mechanical energy, however, it can minimize the depolarizing field energy generated by the unbalanced polarization charges.[22,23] The origin of two c-domains can be correlated with the stress from CFO. Because the PTO matrix is strongly stressed near the CFO rods but weakly stressed far from the rods, the different degrees of strain could induce formation of two PTO domains with different lattice constants. The longer CFO rod length induces a larger concentration of the c_1-domain. Because most of the films contain larger concentration of the c_2-domain, Fig. 1(c) and its inset show the lattice constants and tetragonality (c/a) of the c_2-domain, respectively. The average c/a of 1.045 on STO is larger than that of 1.017 on MgO.[15] Additionally, the 26 nm film produced a larger c/a of 1.067 than the bulk PTO (1.064), revealing an enhanced polarization. However, the compressive strain increases slightly and tetragonality decreases as increasing thickness. The CFO lattice constants shift towards the bulk values while PTO lattice constants deviate as thickness increases. It implies that a competition of strain relaxation exists between these two phases.

The AFM images[16] reveal that the CFO pillars were 20 nm in diameter distributed in a PTO matrix with an average distance of 20 nm for all films. This shows all films have the same densities of nano-rods distributed in a matrix. CFO-PTO films exhibit a higher density of nano-rods than other nanostructures[2,3,17,18] providing a large interface-to-volume ratio to improve stress transmission and increase the surface stress.[24] The length to diameter ratios (aspect ratios) of the 17 nm and 205 nm films were estimated to be 0.85 and 10.3, respectively. Figures 2(a)–2(c), respectively, show the hysteresis loops, the coercive fields (H_C), and the remnant magnetization to saturation magnetization ratios (Mr/M_S) for the films under the in-plane (blue circles) and out-of-plane (red dots) magnetic fields. Comparing with the out-of-plane magnetic anisotropy of the most films, the in-plane preferred anisotropy of the 17 nm film is a result of the in-plane compression induced by the substrate.[20,21] The in-plane H_C remain nearly the same, while the out-of-plane H_C significantly increases as the aspect ratio increases. Strong enhancements in the out-of-plane H_C and Mr/M_S indicate that a spin reorients from the in-plane to out-of-plane direction. The shape of CFO rods and the out-of-plane compressed stress can cause perpendicular anisotropy. To identify the contributions from the shape (filled squares) and strain (opened squares) effects, these two anisotropies were calculated, as shown in Fig. 2(d). Adopting a one-dimensional model of $2\pi(N_X - N_Z)M_S^2$, where N is the demagnetizing factor,[17] shape anisotropies of 1.5×10^5 and

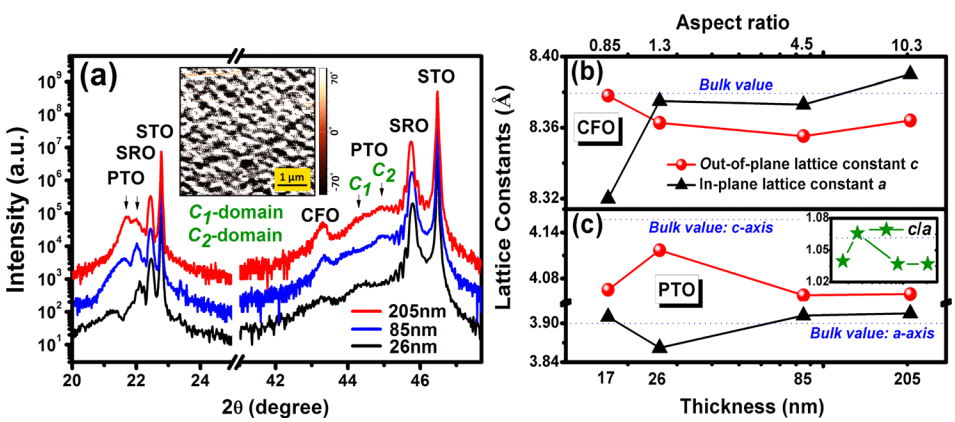

FIG. 1. XRD θ-2θ scan along the surface normal (a) for CFO-PTO films. The c_1 and c_2 domains refer to two PTO domains which are confirmed as vertically polarized by the out-of-plane PFM phase image in the inset of Fig. 1(a). The out-of-plane (red dots) and in-plane (black triangles) lattice constants for CFO (b) and PTO (c) as a function of film thickness, which corresponds to different aspect ratios of CFO rods with the same diameter. The c/a (green stars) shows the tetragonalities of the c_2-domain of PTO in the inset of Fig. 1(c).

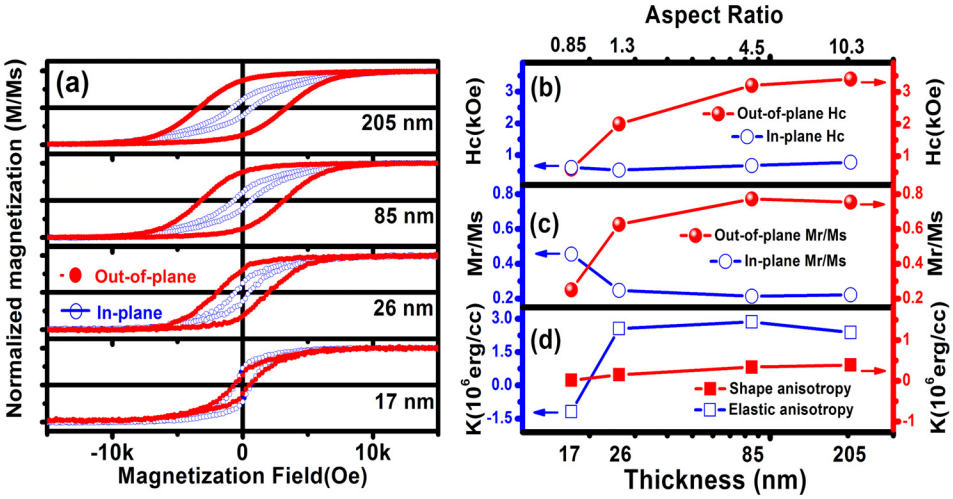

FIG. 2. In-plane (open dot) and out-of-plane (filled dot) magnetic hysteresis loops (a), H_C (b), and Mr/Ms (c) for CFO-PTO films. The calculated shape anisotropy (filled dot) and magnetoelastic anisotropy (open dot) (d) for films of various thicknesses.

3.9×10^5 were estimated for the 26 nm and 205 nm films, respectively. The magnetoelastic anisotropy of the 85 nm film was estimated to be 2.86×10^6 by using the formula of $\frac{3}{2}\lambda_{33}\sigma_{001}$,[17] where λ_{33} and σ_{001} correspond to the magnetostriction coefficient and the out-of-plane stress on CFO, respectively. Therefore, magnetoelastic anisotropy dominates the vertical anisotropy. By contrast, shape anisotropy dominates BFO-CFO film when the aspect ratio is larger than 5.[18] The slight decreases in Mr/M_S and magnetoelastic anisotropy in the 205 nm film are caused by the partial strain relaxation.

To assign the phonon modes, Fig. 3(a) shows the Raman signatures of CFO-PTO films and pure individual films for comparison. After subtracting the substrate signals, the Raman spectra of CFO-PTO films are normalized by Bose factor and fitted with Lorentzian functions within a root-mean square error of ~9.2% as shown in Figs. 3(b) and 3(c). The measurement time of $Z(XY)\bar{Z}$ configuration is four times longer than that of $Z(XX)\bar{Z}$ configuration owing to the small signals in the $Z(XY)\bar{Z}$ configuration. The phonons near 254 cm^{-1} and 367 cm^{-1} in the $Z(XX)\bar{Z}$ spectrum and at 360 cm^{-1} in the $Z(XY)\bar{Z}$ spectrum, showing reduced intensities as the thickness increases, are ascribed to the SRO-A_g and B_{2g} modes, respectively, in accordance with Iliev.[25] According to the $Fd\bar{3}m$ space group of inverse spinel CFO,[26–29] the $A_{1g}(1)$ phonon at 700 cm^{-1} in the $Z(XX)\bar{Z}$ configuration[15,29] and $T_{2g}(1)$ mode near 580 cm^{-1} in the $Z(XY)\bar{Z}$ one are exempted from overlapping with other modes. The B-site phonon at 470 cm^{-1} in the $Z(XX)\bar{Z}$ spectrum, originating from short-range ordering of Co and Fe cations at octahedral sites,[29,30] overlaps with PTO-A_1(3TO) mode for the thinner films. According to the selection rule of the P_{4mm} space group[31–34] for an *c*-polarized tetragonal PTO, only A_1(LO) and B_1 modes[33,35,36] are allowed in the $Z(XX)\bar{Z}$ configurations. However, the A_1(TO) and E(TO) modes including the silent E(4TO) mode are observed. The appearances of E(TO) modes and A_1(TO) modes in $Z(XY)\bar{Z}$ and $Z(XX)\bar{Z}$ configurations, respectively, could be caused by the imperfect *c*-oriented PTO domains or the high NA of objective.[33,37] Additionally, the large interfacial strain could induce local symmetry to break from tetragonal to monoclinic structure, which enables the E(TO) modes allowed in the $Z(XY)\bar{Z}$ configuration.[38] All modes, except

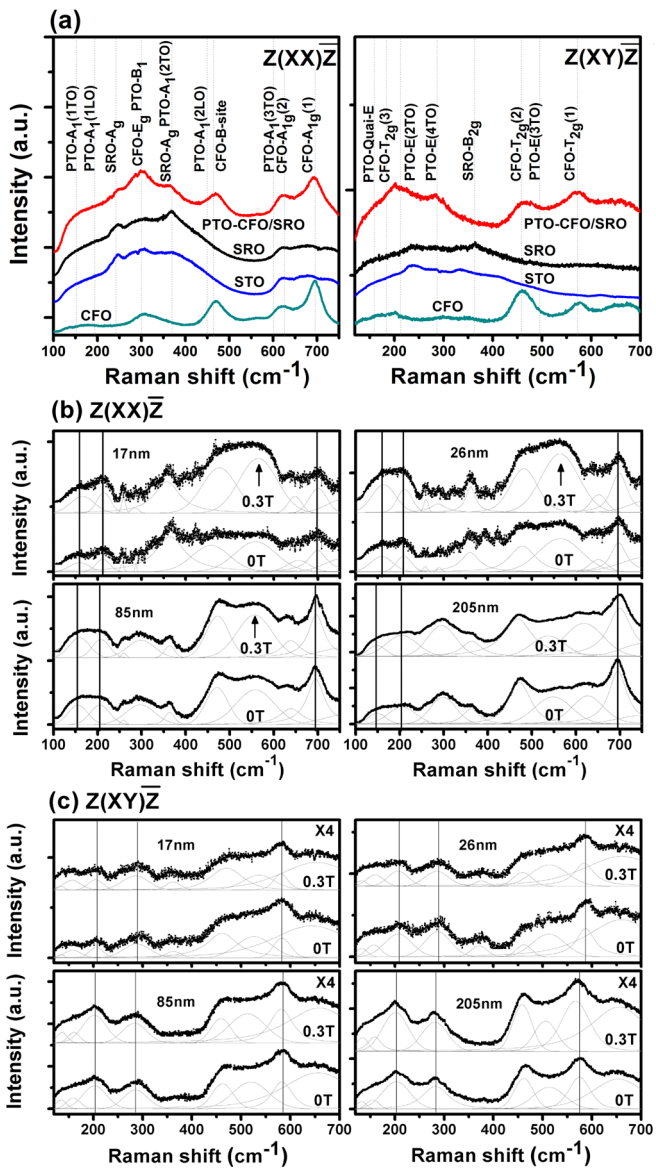

FIG. 3. Phonon assignments (a) for CFO-PTO nanostructures and individual pure films. The polarized Raman spectra of CFO-PTO nanostructures of various thicknesses recorded in the $Z(XX)\bar{Z}$ (b) and $Z(XY)\bar{Z}$ (c) configurations under 0 T (lower line) and 0.3 T (upper line) magnetic fields.

the superposition of phonons (i.e., B_1-symmetry mode overlaps with CFO-E_g mode near 300 cm^{-1}, quasi-E mode overlaps with the $T_{2g}(3)$ mode near 100 cm^{-1} to 180 cm^{-1}, and E(3TO) mode mixes with $T_{2g}(2)$ mode near 500 cm^{-1} to 600 cm^{-1}), are discussed.

Changes of phonon frequencies with thickness can be correlated with strain variations. As the thickness increases, the intensities of $A_{1g}(1)$ and B-site phonons increases in the spectra. The decreased $A_{1g}(1)$ mode frequency consists with the gradually released CFO strain. The CFO-PTO nanostructure has a lower PTO Raman intensity than pure PTO film, which implies the PTO Raman oscillator strength decreases. The larger band gap of PTO[39,40] than that of CFO[41,42] might cause the Raman response function χ'' to decrease. Additionally, high strains and small grains of PTO could cause phonon softening.[43,44] In contrast to the broadening of the $A_1(1LO)$ and $A_1(1TO)$ modes as thickness increases, the spectral lines of E(2TO) and silent E(4TO) modes become sharper. The difference might occur because PTO stress increases along the out-of-plane direction, but slightly relaxes along the in-plane direction since A_1 modes dominate the out-of-plane vibrations and E modes characterize the in-plane vibrations.[45] This is consistent with the decreased $A_1(1TO)$ phonon frequencies and decreased tetragonalities in Fig. 1(c), revealing weakened ferroelectricity in the thicker films. Moreover, the down-shifted CFO-$T_{2g}(1)$ and PTO-E(TO) mode frequencies in the thicker films show the two phases are simultaneously under in-plane tensile stress. However, the contrasting intensity and FWHM variation trends between the CFO-$A_{1g}(1)$ and PTO-A_1 modes reveal the opposite vertical strains between them. These differences might be caused by thermal stress. As samples were cooled from PTO Curie temperature after deposited, the PTO lattice parameters increased (decreased) along the vertical (horizontal) direction, whereas those of CFO decreased in all three directions. Furthermore, the thickness-dependent phonon behaviors in CFO-PTO films differ from those in pure PTO films,[35] which also evidences the coupling from CFO.

By imposing a 0.3 T perpendicular magnetic field, the $A_{1g}(1)$ mode hardens and the $T_{2g}(1)$ phonon softens, particularly for the thicker films, as shown in the upper lines of Figs. 3(b) and 3(c), respectively. Because magnetostriction produces strong out-of-plane compression and slight in-plane expansion in CFO according to the magnetostrictive coefficients, A_{1g} phonon frequency blue shiftes.[15] Because the $T_{2g}(1)$ (582 cm^{-1}) phonon represents the asymmetrical translation movement of FeO_4,[27] the elongated lattices *a* and *b* cause a red-shifted frequency more than the compressed lattice *c* does. Furthermore, the largest up-shift frequency for the 205 nm film in Fig. 4(b) indicates that the higher aspect-ratio rod or strain-relaxed CFO could generate the large magnetostriction. Although the overlapping between $A_1(3TO)$ and B-site phonons causes difficulty in precisely determining the frequencies, the intensity of $A_1(3TO)$ increases under the magnetic fields, as indicated by the arrows in Fig. 3(b). The intensity ratio of $A_1(3TO)$ phonon to B-site phonon increases under the magnetic field, particularly for the thinner films. The enhancements for the thicker films were imperceptible because of the broader FWHM. Additionally, the intensities and frequencies of $A_1(1LO)$ and $A_1(1TO)$ modes also enhance. Hardening of these phonons, although uncommon, can be achieved by controlling epitaxial stress on PTO.[46] Because Raman emission is proportional to the square of spontaneous polarizations by assuming a constant phonon frequency and temperature,[33] the anomalous increased phonon intensities imply that the spontaneous polarizations are enhanced through interfacial coupling with CFO, indicating that ME effect exists. By contrast, the E(2TO) and silent E(4TO) modes either broaden in shape or down shift in frequency under the magnetic field, showing the increased in-plane tensile stress.[46] We notice that the hardened $A_{1g}(1)$ and softened $T_{2g}(1)$ modes of CFO are similar to the behaviors of the A_1 and E modes of PTO, respectively. This strongly suggests these phonons are coupled among one another through anisotropic interfacial stress, as shown in Figs. 5(a) and 5(b). It has been found that the E(2TO) mode hardens and $A_1(1TO)$ mode softens in CFO-PZT bi-layer films under a vertical magnetic field.[13] This indicates that the connected orientations of two phases can cause opposite lattice dynamics. Considering the phonon vibrations, the $A_{1g}(1)$ phonon is related to the $A_1(TO)$ phonon and the $T_{2g}(1)$ mode is more associated with the E-symmetry mode in this study.

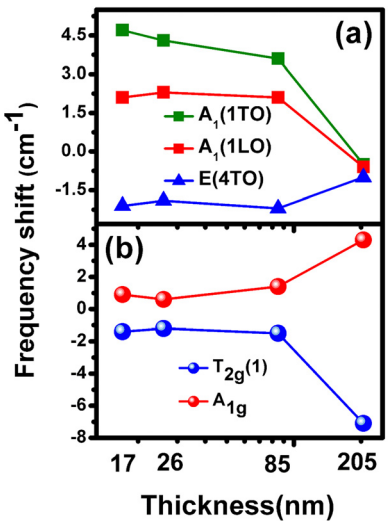

FIG. 4. Magnetic-field induced phonon frequency shifts for PTO-$A_1(1TO)$, $A_1(1LO)$, and E(4TO) modes (a), and CFO-A_{1g} and $T_{2g}(1)$ modes (b).

Because the ME theory predicts that a nanostructure containing the higher aspect-ratio rods can overcome the substrate clamping,[9] the ME strength is expected to increase with thickness. The coupling strength which is probed by the A_1 and E phonon frequency shifts shown in Fig. 4(a) deviates from the theory, especially for 17 nm and 205 nm films. The discrepancy indicates that even though the 205 nm film is highly magnetostrictive, the generated strain cannot be effectively transferred to PTO. The reduced coupling is ascribed to the partial strain-released CFO in 205 nm film, which decreases the stress transmission. Furthermore, the undiminished ME strength of 17 nm film may be associated with the initial out-of-plane elongated lattice, which

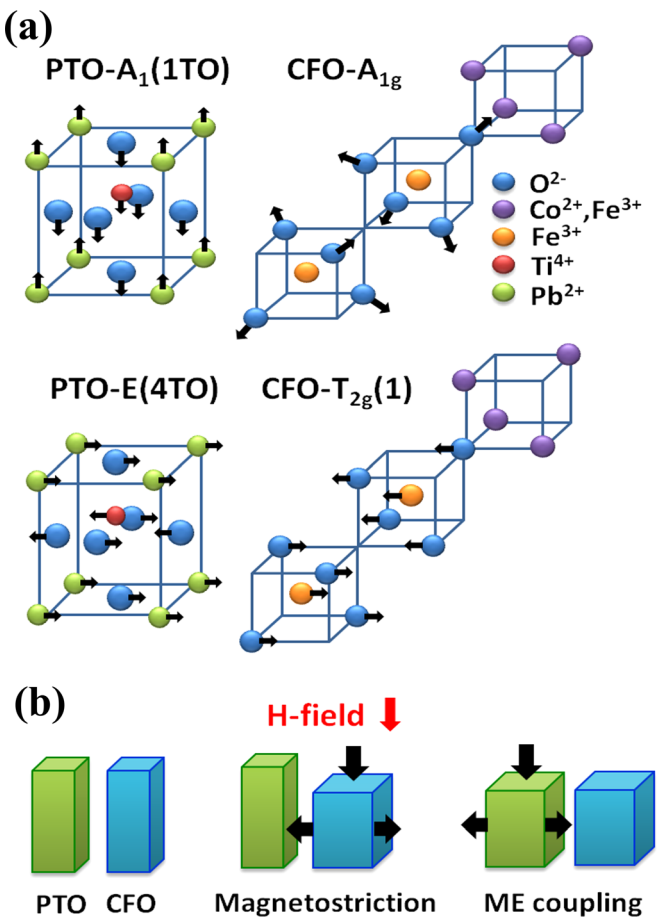

FIG. 5. Phonon mode vibrations (a) according to Verble[27] and Freire[45] and the schematic illustrations of the magnetostrictive effect and ME coupling (b).

although clamped by the substrate, might permit a large vertical compression.[15] The results show that ME coupling is not influenced by solely a single parameter, but that many factors are involved and should be considered. Therefore, we conclude that the interfacial stress dominates ME coupling more than the rod aspect ratio does.

IV. CONCLUSIONS

This study reports on structural, magnetic, and Raman studies of self-assembled CFO-PTO nanostructures. Changes in magnetic anisotropies and phonon behaviors with film thickness are strongly correlated with the anisotropic strain of two phases. Magnetic fields induced opposite phonon frequency shifts between the $A_{1g}(1)$ and $T_{2g}(1)$ modes of CFO and between the A_1 and E modes of PTO, providing evidences for magnetostriction and stress-mediated ME coupling, respectively. Furthermore, the interfacial stress, which dominates ME transmission processes, should be taken into account to improve ME efficiency.

ACKNOWLEDGMENTS

This work was partially supported by National Science Council of Taiwan under Grants NSC-102-2112-M-009-016-MY3 and NSC 100-2112-M-006-002-MY3.

[1]H. Zheng, J. Wang, S. E. Lofland, Z. Ma, L. Mohaddes-Ardabili, T. Zhao, L. Salamanca-Riba, S. R. Shinde, S. B. Ogale, F. Bai, D. Viehland, Y. Jia, D. G. Schlom, M. Wuttig, A. Roytburd, and R. Ramesh, Science **303**, 661 (2004).
[2]Y. H. Hsieh, J. M. Liou, B. C. Huang, C. W. Liang, Q. He, Q. Zhan, Y. P. Chiu, Y. C. Chen, and Y. H. Chu, Adv. Mater. **24**, 4564 (2012).
[3]H. J. Liu, V. T. Tra, Y. J. Chen, R. Huang, C. G. Duan, Y. H. Hsieh, H. J. Lin, J. Y. Lin, C. T. Chen, Y. Ikuhara, and Y. H. Chu, Adv. Mater. **25**, 4753 (2013).
[4]C. W. Nan, G. Liu, Y. Lin, and H. Chen, Phys. Rev. Lett. **94**, 197203 (2005).
[5]S. Geprags, D. Mannix, M. Opel, S. T. B. Goennenwein, and R. Gross, Phys. Rev. B **88**, 054412 (2013).
[6]P. E. Janolin, N. A. Pertsev, D. Sichuga, and L. Bellaiche, Phys. Rev. B **85**, 140401(R) (2012).
[7]G. Bai, X. Gong, Z. G. Liu, Y. D. Xia, and J. Yin, J. Appl. Phys. **112**, 114121 (2012).
[8]G. Liu, C. W. Nan, Z. K. Xu, and H. Chen, J. Phys. D: Appl. Phys. **38**, 2321 (2005).
[9]V. M. Petrov, G. Srinivasan, M. I. Bichurin, and A. Gupta, Phys. Rev. B **75**, 224407 (2007).
[10]T. X Li, M. Zhang, F. J. Yu, Z. Hu, K. S. Li, D. B. Yu, and H. Yan, J. Phys. D: Appl. Phys. **45**, 085002 (2012).
[11]Y. Wang, J. Hu, Y. Lin, and C. W. Nan, NPG Asia Mater. **2**, 61 (2010).
[12]L. Yan, Z. Xing, Z. Wang, T. Wang, G. Lei, J. Li, and D. Viehland, Appl. Phys. Lett. **94**, 192902 (2009).
[13]Z. Li, Y. Wang, Y. Lin, and C. W. Nan, Phys. Rev. B **79**, 180406(R) (2009).
[14]Z. Li, Y. Gao, B. Yang, Y. Lin, R. Yu, and C. W. Nan, J. Am. Ceram. Soc. **94**, 1060 (2011).
[15]C. Y. Tsai, H. R. Chen, F. C. Chang, W. C. Tsai, H. M. Cheng, Y. H. Chu, C. H. Lai, and W. F. Hsieh, Appl. Phys. Lett. **102**, 132905 (2013).
[16]See supplementary material http://dx.doi.org/10.1063/1.4870803 for the Phi-scan measurements of CFO-PTO/SRO/STO(001), which reveals an epitaxial relation of $(001)[101]_{PTO}\|(001)[101]_{CFO}\|(001)[101]_{SRO}\|(001)[101]_{STO}$ and for the AFM topographies of CFO-PTO films of various thicknesses.
[17]H. Zheng, J. Kreisel, Y. H. Chu, R. Ramesh, and L. Salamanca-Riba, Appl. Phys. Lett. **90**, 113113 (2007).
[18]Z. Wang, Y. Li, R. Viswan, B. Hu, V. G. Harris, J. Li, and D. Viehland, ACS Nano **7**, 3447 (2013).
[19]R. Comes, M. Khokhlov, H. Liu, J. Lu, and S. A. Wolf, J. Appl. Phys. **111**, 07D914 (2012).
[20]F. Rigato, J. Geshev, V. Skumryev, and J. Fontcuberta, J. Appl. Phys. **106**, 113924 (2009).
[21]X. S. Gao, D. H. Bao, B. Birajkar, T. Habisreuther, R. Mattheis, M. A. Schubert, M. Alexe, and D. Hesse, J. Phys. D: Appl. Phys. **42**, 175006 (2009).
[22]J. S. Speck and W. Pompe, J. Appl. Phys. **76**, 466 (1994).
[23]S. K. Streiffer, J. A. Eastman, D. D. Fong, C. Thompson, A. Munkholm, M. V. Ramana Murty, O. Auciello, G. R. Bai, and G. B. Stephenson, Phys. Rev. Lett. **89**, 067601 (2002).
[24]M. D. Glinchuk, E. A. Eliseev, A. N. Morozovska, and R. Blinc, Phys. Rev. B **77**, 024106 (2008).
[25]M. N. Iliev, A. P. Litvinchuk, H.-G. Lee, C. L. Chen, M. L. Dezaneti, C. W. Chu, V. G. Ivanov, M. V. Abrashev, and V. N. Popov, Phys. Rev. B **59**, 364 (1999).
[26]J. L. Verble, Phys. Rev. B **9**, 5236 (1974).
[27]P. Chandramohan, M. P. Srinivasan, S. Velmurugan, and S. V. Narasimhan, J. Solid State Chem. **184**, 89 (2011).
[28]O. N. Shebanova and P. Lazor, J. Solid State Chem. **174**, 424 (2003).
[29]M. N. Iliev, D. Mazumdar, J. X. Ma, A.Gupta, F. Rigato, and J. Fontcuberta, Phys. Rev. B **83**, 014108 (2011).
[30]V. G. Ivanov, M. V. Abrashev, M. N. Iliev, M. M. Gospodinov, J. Meen, and M. I. Aroyo, Phys. Rev. B **82**, 024104 (2010).
[31]A. Bartasyte, O. Chaix-Pluchery, J. Kreisel, J. Santiso, M. Boudard, C. Jimenez, A. Abrutis, and F. Weiss, IEEE Trans. Ultrason. Ferroelectr. Freq. Control **54**, 2623 (2007).
[32]G. Burns and B. A. Scott, Phys. Rev. Lett. **25**, 167 (1970).
[33]G. Burns and B. A. Scott, Phys. Rev. B **7**, 3088 (1973).
[34]M. D. Fontana, H. Idrissi, G. E. Kugel, and K. Wojcik, J. Phys.: Condens. Matter **3**, 8695 (1991).
[35]A. Bartasyte, O. Chaix-Pluchery, J. Kreisel, C. Jimenez, F. Weiss, A. Abrutis, Z. Saltyte, and M. Boudard, J. Appl. Phys. **103**, 014103 (2008).

[36]S.-H. Lee, H. M. Jang, S. M. Cho, and G.-C. Yi, Appl. Phys. Lett. **80**, 3165 (2002).
[37]A. Bartasyte, S. Margueron, J. Kreisel, P. Bourson, O. Chaix-Pluchery, L. Rapenne-Homand, J. Santiso, C. Jimenez, A. Abrutis, F. Weiss, and M. D. Fontana, Phys. Rev. B **79**, 104104 (2009).
[38]A. S. Anokhin, Yu. I. Yuzyuk, Yu. I. Golovko, V. M. Mukhortov, and M. El Marssi, J. Appl. Phys. **109**, 074111 (2011).
[39]S. Piskunov, E. Heifets, R. I. Eglitis, and G. Borstel, Comput. Mater. Sci. **29**, 165 (2004).
[40]S. de Lazaro, E. Longo, J. R. Sambrano, and A. Beltran, Surf. Sci. **552**, 149 (2004).
[41]B. S. Holinsworth, D. Mazumdar, H. Sims, Q.-C. Sun, M. K. Yurtisigi, S. K. Sarker, A. Gupta, W. H. Butler, and J. L. Musfeldt, Appl. Phys. Lett. **103**, 082406 (2013).
[42]A. V. Ravindra, P. Padhan, and W. Prellier, Appl. Phys. Lett. **101**, 161902 (2012).
[43]J. A. Sanjurjo, E. L. Cruz, and G. Burns, Phys. Rev. B **28**, 7260 (1983).
[44]K. Ishikawa, K. Yoshikawa, and N. Okada, Phys. Rev. B **37**, 5852 (1988).
[45]J. D. Freire and R. S. Katiyar, Phys. Rev. B **37**, 2074 (1988).
[46]L. Sun, Y. F. Chen, L. He, C. Z. Ge, D. S. Ding, T. Yu, M. S. Zhang, and N. B. Ming, Phys. Rev. B **55**, 12218 (1997).